Phaseless Bi-Polar Planar Near-Field Measurements and Diagnostics of Array Antennas

Robert G. Yaccarino, *Member, IEEE*, and Yahya Rahmat-Samii, *Fellow, IEEE*

***Abstract*— Antenna near-field measurements typically require very accurate measurement of the near-field phase. There are applications where an accurate phase measurement may not be practically achievable. Phaseless measurements are beginning to emerge as an alternative microwave antenna measurements technique when phase cannot be directly measured. There are many important aspects for successful implementation of a phaseless measurement algorithm. This paper presents appropriate phaseless measurement requirements and a phase retrieval algorithm tailored for the bi-polar planar near-field antenna measurement technique. Two amplitude measurements and a squared amplitude optimal sampling interpolation method are integrated with an iterative Fourier procedure to first retrieve the phase information and then construct both the far-field pattern and diagnostic characteristics of the antenna under test. In order to critically examine the methodologies developed in this paper, phaseless measurement results for two different array antennas are presented and compared to results obtained when the near-field amplitude and phase are directly measured.**

***Index Terms*—Antenna diagnostics, antenna measurements, bi-polar near-field, phaseless measurement, phase retrieval.**

I. Introduction

NEAR-FIELD antenna measurement methods [1], [2], in contrast to conventional far-field methods, make use of a measuring probe in the radiating near-field region of the antenna under test (AUT). The far-field pattern of the AUT, not being directly measured, must be indirectly computed from the measurements made in the near-field region. For planar near-field measurements, a Fourier transform of the complex (amplitude and phase) near-field data is required to obtain the far-field pattern. A very accurate measurement of the near-field phase is typically required. There are applications, however, where an accurate phase measurement may not be practically achievable. For example, in high-frequency applications the accuracy of the phase measurement might be limited by the positional tolerances of the measuring probe. The prohibitive cost of vector measurement equipment can also be a substantial impediment to obtaining any phase information.

Phaseless measurement methods are beginning to emerge as an alternative microwave antenna measurements technique when it is impractical to directly measure phase. The process of recovering the phase is known as the "phase retrieval" problem. A variety of algorithms, almost exclusively numerical in nature, have been investigated in recent years for the phase retrieval problem at microwave and millimeter wave frequencies. Excellent overviews of both the underlying mathematical basis for the phase retrieval problem and a comparison of various practical algorithms are contained in [3], [4]. A number of methods have focused on iterative Fourier algorithms with enforcement of the measured phaseless data constraints at each step. Examples of techniques in this category include the error-reduction (Gerchberg–Saxton) [5], input–output [4], and Misell [6] algorithms. These techniques all originated in the optical regime and require amplitude measurements in the far-field region, which, of course, is impractical from the near-field antenna measurements perspective.

The plane-to-plane [7] algorithm, an iterative Fourier technique, was specifically formulated for the case of planar near-field antenna measurements and, therefore, admits the same measurement apparatus for both required phaseless near-field antenna measurements. In recent years, an approach to the phase retrieval problem as a nonlinear inverse problem [8] has gained attention. In this technique, an appropriately defined functional based on the known squared amplitude near-field data is numerically minimized. This approach to the phase retrieval problem is also amenable to the planar near-field antenna measurement scenario. With few exceptions, however, these techniques have been applied to simulations and measurements in which the near-field measurement planes were separated by a considerable electrical distance.

There are many important aspects for successful implementation of a phaseless measurement algorithm. This paper presents appropriate phaseless measurement requirements and a phase retrieval algorithm tailored for the bi-polar planar near-field antenna measurement technique. Two amplitude measurements and a squared amplitude optimal sampling interpolation method are integrated with an iterative Fourier procedure to first retrieve the phase information and then construct both the far-field pattern and diagnostic characteristics of the AUT. In order to critically examine the algorithms presented in [9] for antenna imaging applications and refined in this paper for phaseless array diagnostics, phaseless measurement results for two distinct examples, the phase retrieval of a near-circular aperture array antenna and the phaseless diagnostics of a masked elliptical aperture array antenna, are presented and compared to results obtained when the near-field amplitude and phase are directly measured.

The remainder of this paper is organized as follows. Section II briefly describes the bi-polar planar near-field antenna measurement technique. Section III provides an overview of the essential aspects of the optimal sampling

Manuscript received June 24, 1997; revised June 2, 1998.

The authors are with the Department of Electrical Engineering, University of California, Los Angeles, Los Angeles, CA 90095 USA.

Publisher Item Identifier S 0018-926X(99)04437-3.

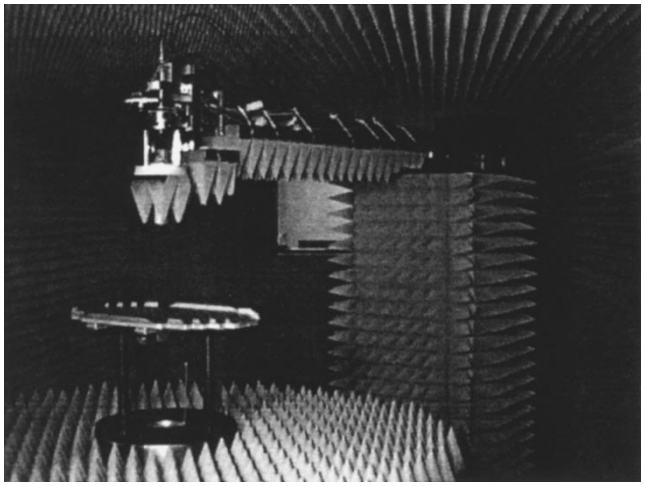

Fig. 1. The UCLA bi-polar planar near-field antenna measurement range.

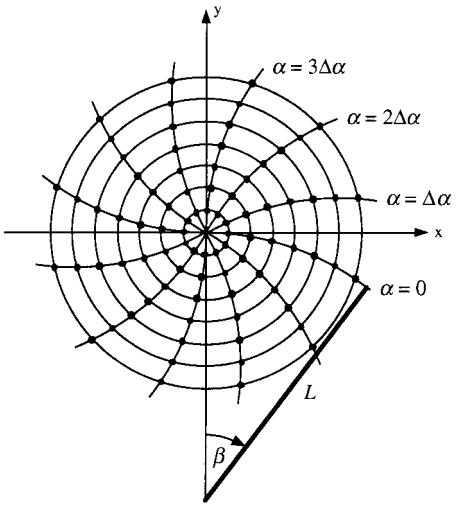

Fig. 2. Bi-polar planar near-field sample arrangement and coordinate system (β, α). L is the length of the probe arm.

interpolation (OSI), a component of the bi-polar phase retrieval algorithm. A step-by-step guide to the bi-polar phase retrieval algorithm is given in Section IV. This section also details two critical components of the process: squared amplitude OSI and Fourier iteration. Section V contains measurement results for two different array antennas in order to illustrate the applicability and accuracy of the phase retrieval algorithm. Finally, some concluding remarks are given in Section VI.

II. Bi-Polar Planar Near-Field Antenna Measurements at UCLA

The concept, design, and implementation of the bi-polar planar near-field antenna measurement technique has been extensively described by the authors in previous publications [10]–[12]. It has been demonstrated that this measurement technique is a highly accurate and cost-effective means for performing antenna measurements and diagnostics. Among the many attractive features of this bi-polar technique are a large scan plane size requiring minimal "real-estate" investment and a simple mechanical implementation requiring only rotational motions.

The UCLA bi-polar planar near-field scanner (shown installed in an anechoic chamber in Fig. 1) consists of an AUT mounted to a positioner that rotates about one axis and a probe antenna mounted to a probe arm that rotates about a second axis. The combination of these two rotational motions results in near-field data collected on concentric circular rings with data samples located at the intersection with circular radial arcs. The bi-polar sampling distribution, shown in Fig. 2, arises from a repeated measurement sequence in which the AUT rotates through a full revolution followed by an incremental rotation of the probe arm away from the scan plane center. This sampling distribution is described by the independent coordinates (β, α) where β is the angle the probe arm makes with the positive y axis and α is an azimuthal-like angle which remains constant along each circular radial arc. The probe arm length L, a parameter of the coordinate system, determines the radius of the circular radial arcs. The scan plane radius a, a parameter of the measurement, is determined by the maximum angular extent of the probe arm $\beta_{\max}$.

The scanner's robotic positioning system and programmable motion-control software permit considerable flexibility with respect to the sample arrangements which may be acquired [13]. For example, if the probe arm angle β is incremented uniformly one obtains concentric rings spaced nonuniformly in the polar coordinate ρ, however, on the other hand, if the probe arm angle β is incremented nonuniformly (in a prescribed fashion) one obtains concentric rings uniformly spaced in ρ. The number of near-field samples on a measurement ring may also be varied from inner to outer ring to prevent oversampling of the near-field near the scan plane center. Interestingly enough, a bi-polar linear spiral scan can also be achieved through the simultaneous rotation of the AUT and probe arm [14].

III. Optimal Sampling Interpolation of Bi-Polar Near-Field Data

Planar near-field antenna measurement techniques require a Fourier transform of the complex (amplitude and phase) near-field data to obtain the far-field pattern of the AUT. It is usually desirable, from a computational perspective, to employ a fast Fourier transform (FFT) for both the near-field to far-field transformation (with correction for the measuring probe) [15] and for antenna holographic diagnostics [16]. The FFT, however, requires rectangularly distributed data samples. The direct application of the FFT to the bi-polar near-field sample distribution, therefore, is not automatic. Other options are available for computing the far-field pattern directly from the bi-polar near-field samples, for example, the Jacobi-Bessel and Fourier-Bessel transforms [11]. In most cases, however, these techniques are more computationally demanding than the FFT.

To exploit the computational advantages of the FFT, the bi-polar near-field samples need to be converted to a rectangularly regularized format. An OSI algorithm [11], [17] is employed for this purpose for several reasons, the most notable of which are the proper determination of the bi-polar sample spacings (which may be considerably relaxed beyond the

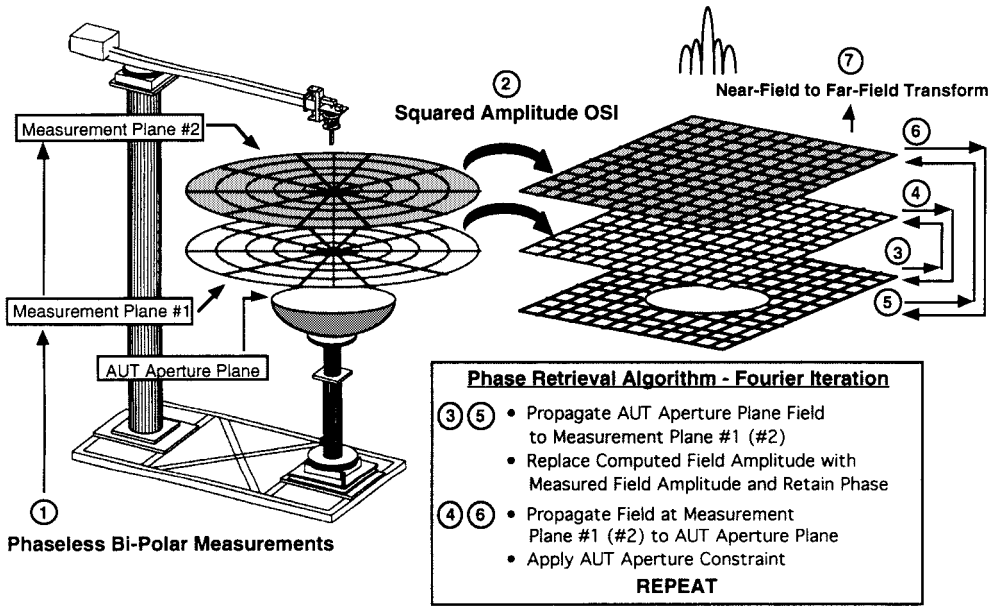

Fig. 3. Bi-polar planar near-field phase retrieval algorithm.

universally considered maximum sample spacing of $\lambda/2$) and the accurate recovery of plane-rectangular samples from a minimum number of bi-polar samples.

The OSI technique considers the AUT a finite radiating structure with limited spatial bandwidth whose extent depends only on the overall dimensions of the AUT. An appropriate representation for the radiated near field is then a cardinal series expansion. The properties of the sampling functions, however, suggest the use of a central interpolation formula in which only a limited number of samples in the vicinity of the desired output sample are utilized. This, of course, implies the introduction of truncation error. The problem at hand is then, given the bandwidth, sample spacing, and the number of retained samples, to find an approximation function for which the maximum relative error is a minimum. The required sample spacings, including an oversampling factor χ, and the approximating functions for the plane-polar technique, corresponding to linear (radial) and circular (azimuthal) domains, have been detailed [17].

The interpolation of the bi-polar near-field samples into a plane-rectangular format given the surrounding bi-polar samples, for the case in which the bi-polar measurement rings are uniformly spaced in the polar coordinate ρ, is calculated using

$$\mathbf{b}(s,\alpha) = \sum_{n=n_o-q+1}^{n_o+q} \sum_{m=m_o-p+1}^{m_o+p} \mathbf{b}(n\Delta s, m\Delta\alpha_n)\Omega\left(\Psi^1_{mn}\right) \times D_{M'_n}\left(\Psi^1_{mn}\right)\Omega\left(\Psi^2_{mn}\right)\operatorname{sinc}\left[\frac{\pi}{\Delta s}\Psi^2_{mn}\right] \tag{1}$$

where $\mathbf{b}$ is the vector output of the measuring probe, $s = \rho/d$ where d is the distance between the AUT and the probe, (n_o, m_o) are the indexes of the near-field sample nearest (on the left) to the desired output sample, $2q$ and $2p$ are, respectively, the number of retained radial arc and azimuthal samples, Δs is the radial sample spacing of the measurement rings, $\Delta\alpha_n$ is the azimuthal sample spacing on ring n, Ω is the Chebychev convergence function [17], D_M is the Dirichlet interpolation function [17] where M'_n is related to the number of samples on the nth ring, and

$$\Psi^1_{mn} = \alpha - m\Delta\alpha_n \qquad \Psi^2_{mn} = s - n\Delta s \tag{2}$$

A rigorous discussion of sampling requirements in the bi-polar coordinates is found in [10] and is based on sampling requirements in the plane-polar coordinates [17]. The OSI interpolation formula (1) takes slightly different forms when the bi-polar sampling is performed in the "native" bi-polar coordinates (β, α) [11] and for bi-polar linear spiral sampling [14].

IV. Bi-Polar Phase-Retrieval Algorithm

A phase retrieval algorithm related to the plane-to-plane technique [7] has been developed for use with the bi-polar planar near-field measurement system. An important requirement of this algorithm is its applicability to *practical* near-field range implementations, which typically require both the AUT to measurement plane *and* measurement plane to measurement plane (multiple phaseless near-field measurements are typically required for phase retrieval) separation to be on the order of just a few wavelengths (contrast this with the $O(1000\lambda)$ separations typical in optical applications of phase retrieval).

The objective of this section is to clearly outline the procedural steps relating to both the phaseless bi-polar measurement requirements and the implementation of the phase retrieval algorithm. A pictorial representation of the bi-polar phase retrieval algorithm, which appears in Fig. 3, will assist in illustrating this process.

Phaseless bi-polar measurements (step 1) are obtained for two different positions of the measuring probe with respect

to the AUT aperture plane. The near-field amplitude data, on each of these measurement planes, is acquired in accordance with the sampling requirements to be described in the next subsection. The UCLA bi-polar scanner can conveniently acquire data on these two measurement planes because of the automated vertical travel built into the probe assembly. In addition, the rotational capabilities of the probe allow the principal polarization of the AUT to maintain orientation with that of the probe during the duration of the measurement.

A "squared amplitude OSI" (step 2) is used to interpolate the phaseless bi-polar measurement data on each plane to a rectangularly regularized format. This is an important step in the algorithm and the critical considerations behind interpolation of the squared-amplitude data are detailed in the next subsection. The squared-amplitude OSI is followed by formation of the amplitude function from the rectangularly regularized squared amplitude data. The amplitude data on each measurement plane along with knowledge of the aperture size and shape (referred to as the "object" or "aperture" constraint) comprise the inputs to the Fourier iteration (steps 3–6) used for the phase retrieval. The details of the Fourier iteration are described in the second subsection.

The product of the Fourier iteration is the complex near-field distribution on the AUT aperture plane and each of the two measurement planes. The Fourier iteration ensures (assuming successful retrieval of the phase) that the complex field distribution on these three planes are related by the Fourier transform. This relationship allows the far-field pattern of the AUT to be computed from the complex field distribution on any one of these three planes (step 7), using standard planar near-field techniques [15].

A. Squared Amplitude OSI

The phase-retrieval algorithm requires interpolation of the phaseless bi-polar near-field measurement data on each measurement plane to a rectangularly regularized format such that an efficient FFT can be used for the subsequent Fourier iteration. The motivation for interpolation of the *squared* amplitude data stems from the Fourier convolution theorem. This theorem ensures that if g (denoting the complex near-field data) is a bandlimited function then so is the squared modulus $|g|^2$, but to a band *twice* that of g. A similar statement, however, cannot be made for the modulus $|g|$. This statement is expressed mathematically as

$$\begin{aligned} &\text{If } g(x) \rightarrow G(k) \quad \text{then } g^*(x) \rightarrow G^*(-k) \\ &\text{and} \quad |g(x)|^2 = g(x)g^*(x) \rightarrow G(k) \otimes G^*(-k) \end{aligned} \tag{3}$$

where G is the Fourier transform of g, g^* is the complex conjugate of g, and $\otimes$ is the convolution operator. It has been demonstrated that the near-field of a radiating antenna, after extraction of an appropriate phase factor, is quasi-bandlimited [17] and, hence, the squared amplitude data is quasi-bandlimited. This bandlimitedness allows a component of the squared amplitude data to be interpolated and this interpolation is performed using OSI [11], [17] as

$$\begin{aligned} |b(s,\alpha)|^2 = &\sum_{n=n_o-q+1}^{n_o+q} \sum_{m=m_o-p+1}^{m_o+p} |b(n\Delta s, m\Delta\alpha_n)|^2 \Omega\big(\Psi^1_{mn}\big) \\ &\times D_{M'_n}\big(\Psi^1_{mn}\big)\Omega\big(\Psi^2_{mn}\big)\,\mathrm{sinc}\Big[\frac{\pi}{\Delta s}\Psi^2_{mn}\Big]. \end{aligned} \tag{4}$$

Finally, since the squared amplitude data is bandlimited to a band twice that of an equivalent amplitude and phase measurement, the required bi-polar sampling rate is *twice* that of the equivalent amplitude and phase measurement. This sampling rate has been thoroughly examined in [17]. For practical applications, however, the bandwidth properties of the squared amplitude data would typically permit relaxation of this sampling requirement.

B. Fourier Iteration

An initial guess for the amplitude and phase in the aperture plane of the AUT is made and truncated to the known physical extent of the AUT. This estimate is then propagated, using plane wave spectrum techniques [18] implemented by FFT out to the first measurement plane. An error metric at this measurement plane is then computed by summing the squared difference of the calculated modulus $|F_{i,j}|$ and measured modulus $M_{i,j}$ at each point (i,j) on the measurement plane. This error metric, which represents a conventional sum squared error of the field amplitude values, mathematically takes the form

$$\varepsilon = \frac{\sum_{i,j}(|F_{i,j}| - M_{i,j})^2}{\sum_{i,j} M^2_{i,j}}. \tag{5}$$

The computed error metric is stored, the measured modulus replaces the calculated modulus, and the result is propagated back to the AUT aperture plane.

The calculated amplitude and phase at the AUT aperture plane is again truncated to the known physical extent of the AUT and the result is propagated out to the second measurement plane. An error metric identical to that computed at the first measurement plane is calculated and stored, the measured modulus replaces the calculated modulus, and result is propagated back to the AUT aperture plane, where the calculated amplitude and phase is again truncated to the known physical extent of the AUT.

The computed error metrics on the two measurement planes at this point are examined to determine whether iterations should continue. Appropriate stopping criteria include both an absolute error limit and an error convergence limit. If a stopping criterion is met then the retrieved amplitude and phase on the AUT aperture plane and the two measured planes are stored and the iterations terminate. If a stopping criterion is not met then the process is repeated until a stopping criterion is met.

V. Measurement Results

One of the principal contributions of this paper is to demonstrate the applicability of the bi-polar planar near-field phase retrieval algorithm using both realistic near-field measurement geometrical configurations and actual measurement data. To accomplish this task and to illustrate the success achieved in implementing this algorithm, bi-polar near-field

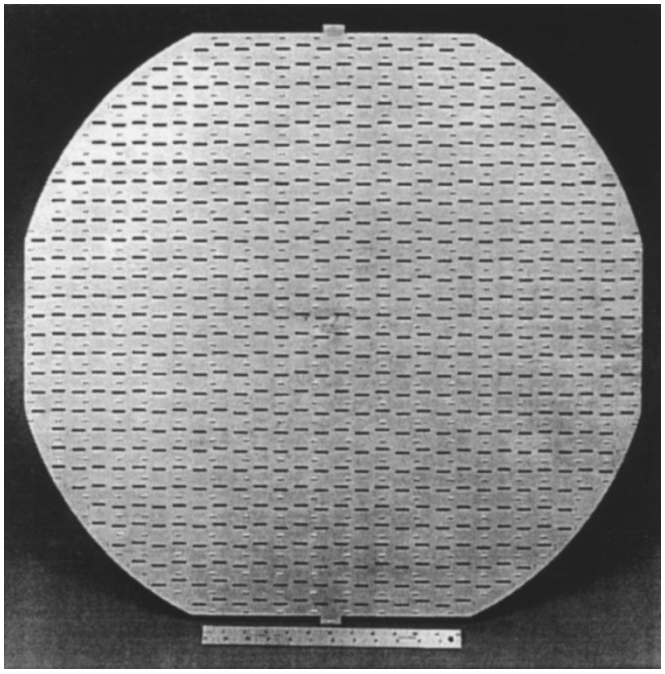

Fig. 4. X-band planar waveguide-fed slot array antenna with nearly circular aperture.

TABLE I
BI-POLAR PLANAR NEAR-FIELD PHASE RETRIEVAL MEASUREMENT PARAMETERS AT 9.375 GHz

	Measurement #1	*Measurement #2*
No. Rings	85	99
No. Samples per Ring	9...313	9...305
No. Samples	20434	22288
Azimuthal Sampling ($\Delta\alpha$)	40.000°...1.722°	40.000°...1.180°
Radial Sampling ($\Delta\rho$)	0.227 λ	0.227 λ
Antenna - Probe Separation (d)	6.255 λ	8.836 λ
Probe Arm Length (L)	41.303 λ	41.303 λ
Scan Plane Radius (a)	19.318 λ	22.500 λ

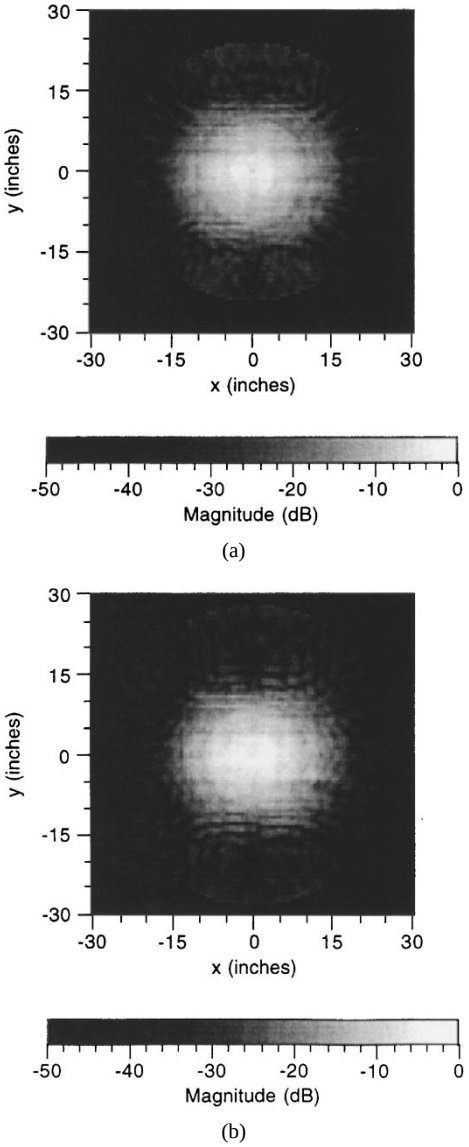

Fig. 5. Magnitude of the measured bi-polar planar near-field data at (a) $d = 6.255\lambda$ and (b) $d = 8.836\lambda$.

measurement results for two different array antennas are presented. The distinct features of these antennas are discussed in the following two subsections. These two example cases, which focus both on far-field pattern construction and antenna diagnostics, provide a solid foundation for exercising the robustness of the bi-polar phase retrieval algorithm.

A. Phase Retrieval of a Near-Circular Aperture Array Antenna

The phase retrieval algorithm has been applied to phaseless bi-polar planar near-field measurement data for the waveguide-fed slot array antenna of Fig. 4. This antenna operates at 9.375 GHz and has a nearly circular aperture measuring 23.0λ (H-plane) $\times 21.4\lambda$ (E-plane). The antenna has 764 radiating slots arranged on an 0.76λ (H-plane) $\times\ 0.70\lambda$ (E-plane) lattice.

A summary of the bi-polar near-field measurement parameters on each of the two measurement planes is provided in Table I. Amplitude and phase were measured on each plane so that phase retrieval results could be compared to results obtained when the amplitude and phase are retained in the data processing. The near-field sampling rate for the measurements was *twice* the sampling rate which would have been used for an equivalent amplitude and phase measurement. The measurement plane separation was 2.581λ and both measurements were configured to yield a valid angle of $\theta_v = 50^\circ$ $(\sin(\theta_v) = 0.766)$.

The bi-polar near-field data on each measurement plane was interpolated using the squared amplitude OSI of (4) to a 128 $\times$ 128 rectangular grid of samples with sample spacings of $\Delta x = \Delta y = 0.485\lambda$. The squared amplitude OSI was performed using a 10 $\times$ 10 patch $(2p = 2q = 10)$ of retained samples. Fig. 5 shows the magnitude of the measured near-field data on each of the two measurement planes. The similarity of the near-field amplitude data on the two measurement planes is a result of their limited separation and, in general, makes the phase retrieval process more difficult.

The phase-retrieval algorithm was initiated with a pseudo-random (± 3 dB amplitude, $\pm 30^\circ$ phase, uniformly distributed) estimate for the field in the aperture of the AUT. This initial estimate of the aperture plane fields was intentionally chosen to exercise the robustness of the algorithm. The phase retrieval

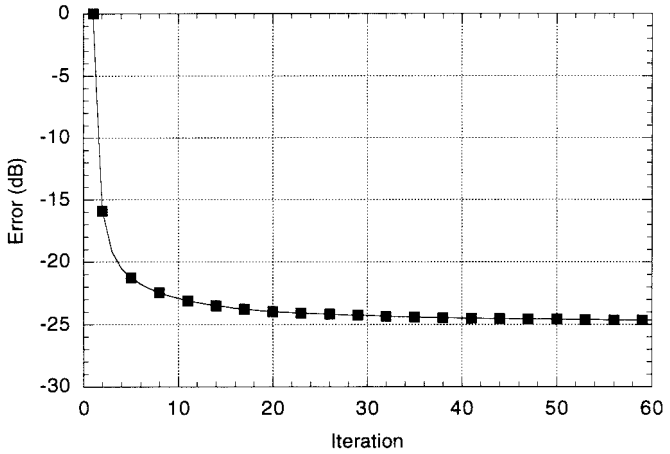

Fig. 6. Phase retrieval error metric versus iteration number on the measurement plane $d = 6.255\lambda$.

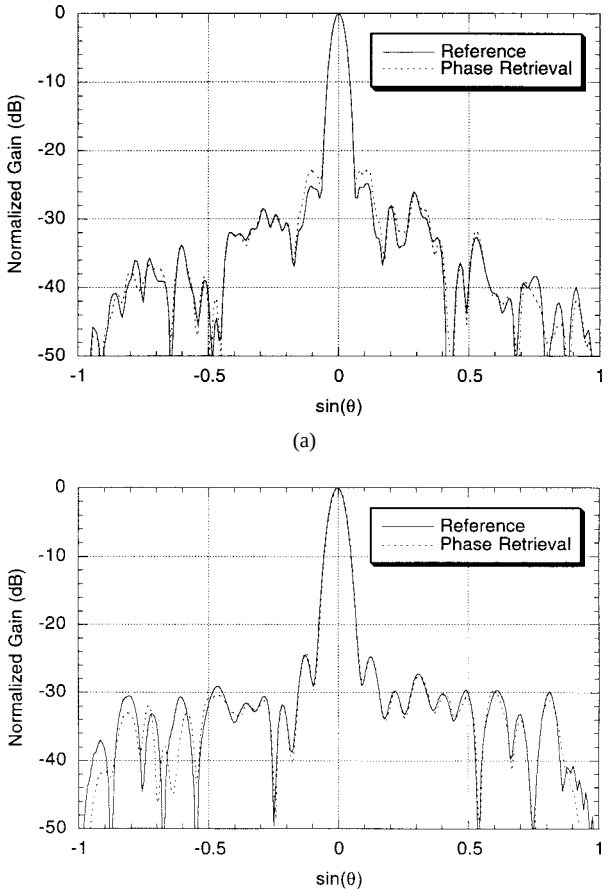

Fig. 7. Comparison of (a) H-plane and (b) E-plane principal plane far-field patterns obtained from a reference (amplitude and phase) measurement and phase retrieval. Valid angle is $\sin(\theta_v) = 0.766$.

algorithm terminated at 134 iterations at which point the error metric, computed using (5), failed to decrease further. A plot of the normalized error versus the first 60 iterations is shown in Fig. 6. The error metric was reduced by 22.9 dB after just ten iterations beyond, which it tended to decrease slowly (reduced by 24.9 dB at algorithm termination).

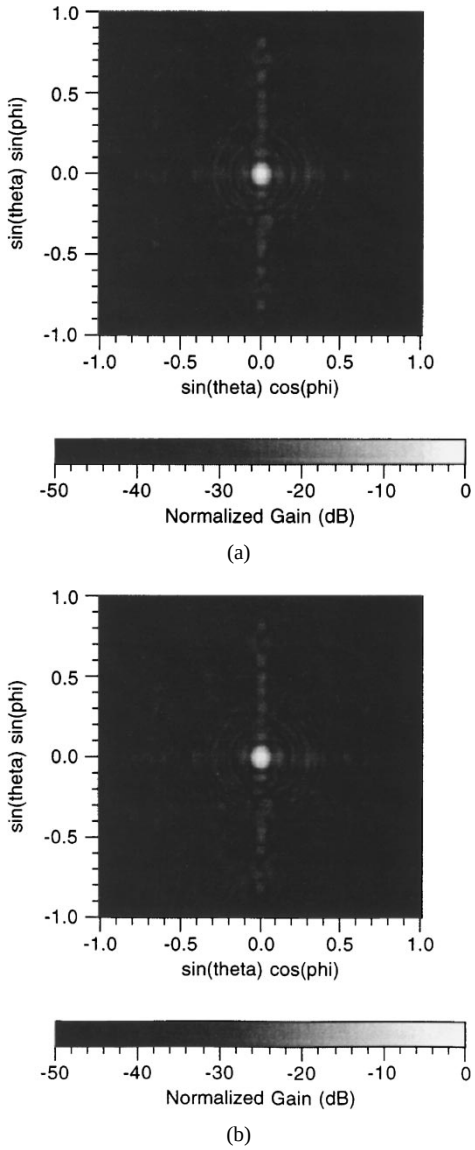

Fig. 8. Far-field patterns obtained from (a) amplitude and phase measurement and (b) phase retrieval.

A 256 × 256 point FFT was used to compute the probe-corrected far-field pattern from the phase retrieval near-field data. A comparison of the H-plane and E-plane patterns of the waveguide-fed slot-array antenna obtained from phase retrieval and from processing utilizing the measured near-field amplitude *and* phase (reference) are shown in Fig. 7. The E-plane results are excellent with regard to both wide-angle and low-pattern level. The H-plane results are also excellent, however, the shouldering effect on the main beam is not accurately reflected. The far-field pattern over the entire spectral region for the case when amplitude and phase are retained in the processing and for the phase retrieval are shown in Fig. 8. These plots demonstrate that the far-field pattern obtained from phase retrieval has been reproduced accurately over the entire spectral region. Table II contains a comparison of several commonly reported far-field pattern statistics for the reference and phase retrieval cases. The pattern statistics confirm that the phase retrieval process has accurately reproduced the reference

TABLE II
FAR-FIELD PATTERN STATISTICS FOR THE WAVEGUIDE-FED SLOT ARRAY ANTENNA

	Reference	*Phase Retrieval*
H-plane Beamwidth	2.90°	2.90°
E-plane Beamwidth	3.43°	3.39°
Directivity	35.54 dB	35.56 dB
Average Sidelobe Level	-44.99 dB	-44.94 dB
Peak Sidelobe Level	-24.46 dB	-22.68 dB

Note: Average sidelobe level is defined to be a measure of the power in the pattern excluding a 10 degree one-sided cone about the main beam.

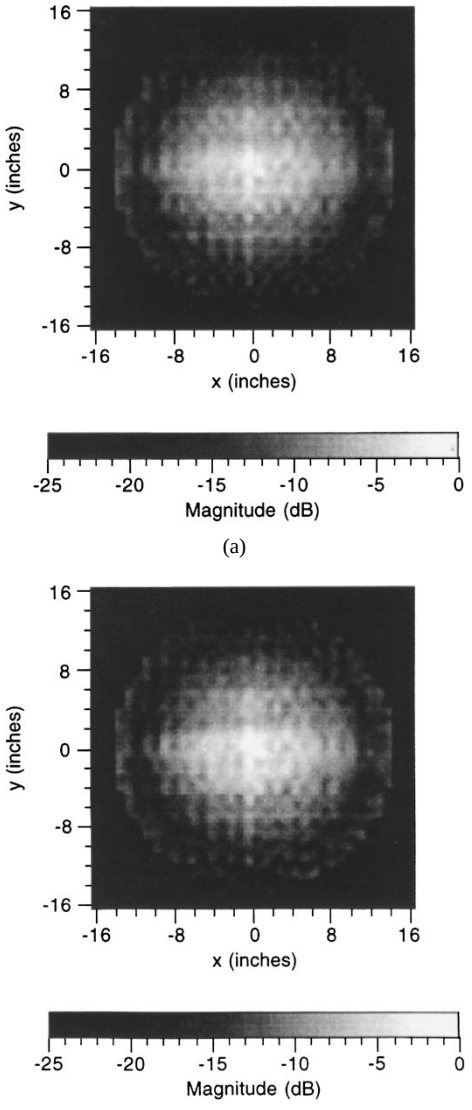

Fig. 9. Holographic image of aperture plane magnitude obtained from (a) amplitude and phase measurement and (b) phase retrieval.

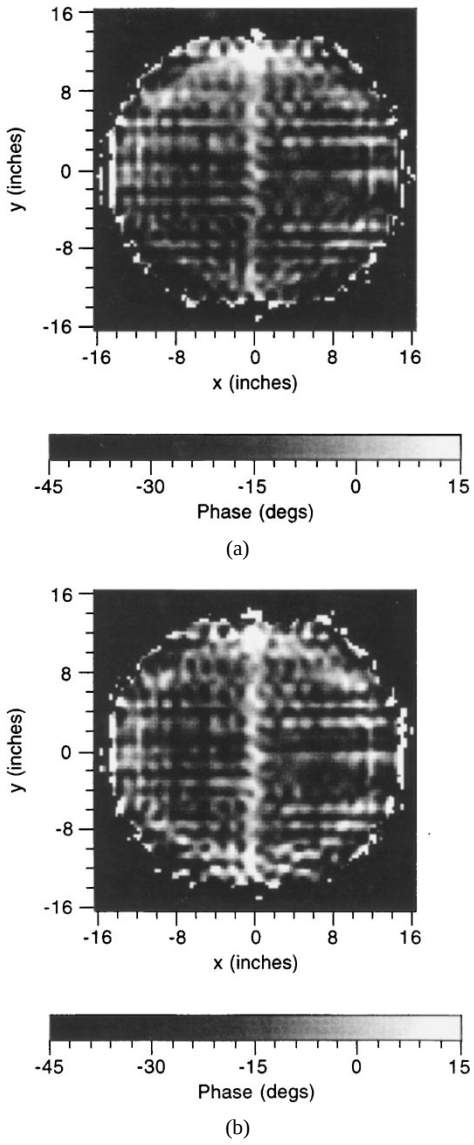

Fig. 10. Holographic image of aperture plane phase obtained from (a) amplitude and phase measurement and (b) phase retrieval.

far-field pattern. The discrepancy in the peak sidelobe level is due to the higher "shoulders" adjacent to the main beam produced by the phase retrieval in the H-plane pattern.

Microwave holographic images of the antenna aperture plane fields have been produced for both the reference and phase retrieval cases to assess the quality of the images reconstructed from phaseless bi-polar near-field measurement data. The holographic images were computed by FFT from the probe-corrected plane wave spectra. The plane wave spectra were zero-padded before application of the FFT in order to produce images with sample spacings of $\Delta x = \Delta y = \lambda/4$. A comparison of the aperture plane magnitude image for the reference and phase retrieval cases is shown in Fig. 9. The aperture plane phase image comparison is shown in Fig. 10. A comparison of the reference and phase retrieval images indicates that an accurate reconstruction of the aperture plane fields from the phaseless bi-polar near-field data has been obtained.

B. Phaseless Diagnostics of a Masked Elliptical Aperture Array Antenna

The phase retrieval algorithm has been applied to phaseless bi-polar near-field measurement data for the waveguide-fed slot array antenna of Fig. 11. This antenna operates at 9.3 GHz and has an elliptical aperture measuring 14.8λ (H-plane)$\times$ 8.7λ (E-plane), an aperture considerably smaller than for the AUT of the prior example. The antenna has 196 radiating slots

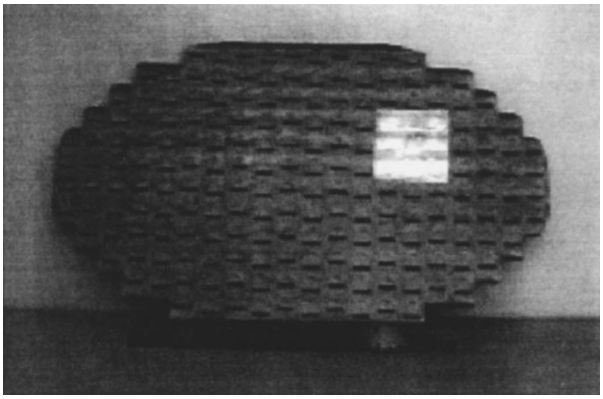

Fig. 11. X-band planar waveguide-fed slot array antenna with elliptical aperture. An aperture anomaly has been introduced by using aluminum tape to mask a 3 × 3 patch of slots in the upper right-hand quadrant.

TABLE III
BI-POLAR PLANAR NEAR-FIELD PHASE RETRIEVAL MEASUREMENT PARAMETERS AT 9.3 GHz

	Measurement #1	*Measurement #2*
No. Rings	81	106
No. Samples per Ring	9...209	5...205
No. Samples	13466	16807
Azimuthal Sampling ($\Delta\alpha$)	40.000°...1.723°	72.000°...1.756°
Radial Sampling ($\Delta\rho$)	0.217 λ	0.217 λ
Antenna - Probe Separation (d)	4.728 λ	7.288 λ
Probe Arm Length (L)	40.972 λ	40.972 λ
Scan Plane Radius (a)	17.609 λ	23.044 λ

arranged on an 0.74λ (H-plane) × 0.69λ (E-plane) lattice. An anomaly in the aperture distribution has been induced by using aluminum tape to mask a 3 × 3 patch of slots in the upper right-hand quadrant of the antenna.

A summary of the bi-polar near-field measurement parameters on each of the two measurement planes is provided in Table III. As in the prior example, amplitude and phase were measured on each plane for the purpose of establishing a comparative reference and the near-field sampling rate for the measurements was *twice* the sampling rate which would have been used for an equivalent amplitude and phase measurement. The measurement plane separation was 2.560λ and both measurements were configured to yield a valid angle of $\theta_v = 65°$ $(\sin(\theta_v) = 0.906)$.

A squared amplitude OSI of the phaseless bi-polar near-field measurement data was used to render a plane-rectangular data format identical to that of the prior example. Fig. 12 shows the magnitude of the measured near-field data on each of the two measurement planes. The similarity of the near-field amplitude data on the two measurement planes and the absence of a pronounced signature due to the induced aperture anomaly should be noted.

As in the prior example, the phase retrieval algorithm was initiated with a pseudo-random (±3 dB amplitude, ±30° phase, uniformly distributed) estimate for the field in the aperture of the AUT. *No a priori knowledge* of the induced aperture anomaly was assumed. The phase-retrieval algorithm terminated at 104 iterations at which point the error metric

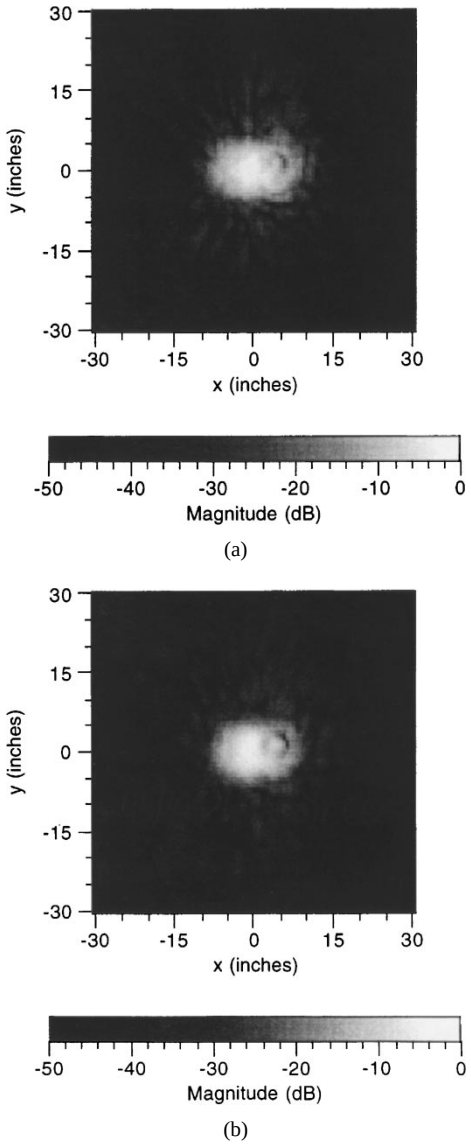

Fig. 12. Magnitude of the measured bi-polar planar near-field data at (a) $d = 4.728\lambda$ and (b) $d = 7.288\lambda$.

of (5), which exhibited the same characteristic profile as that shown in Fig. 6 for the prior example, failed to decrease further. The error metric was reduced by 23.8 dB after just ten iterations beyond which it tended to decrease slowly (reduced by 27.2 dB at algorithm termination).

A comparison of the probe-corrected H-plane and E-plane patterns of the waveguide-fed slot array antenna obtained from phase retrieval and from processing utilizing the measured near-field amplitude *and* phase (reference) are shown in Fig. 13. The H-plane results are excellent with regard to both wide-angle and low-pattern level. The E-plane results are also excellent with perhaps the exception of the region $\sin(\theta) > 0.4$, however, it is noted that the pattern levels here are relatively low. The pattern of the array with no aperture blockage (obtained from a separate amplitude and phase measurement) is also provided as means for establishing a measure of the pattern "disruption" induced by this artificial anomaly. Table IV contains a comparison of far-field pattern

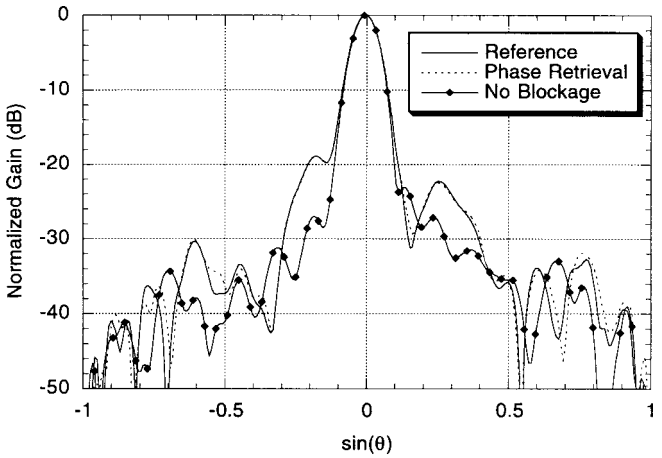

(a)

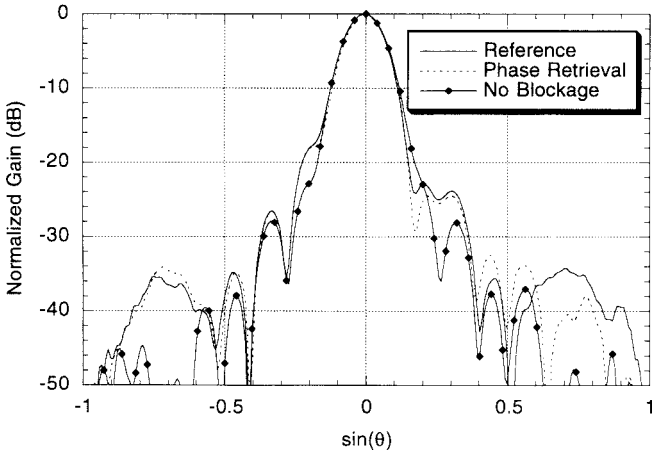

(b)

Fig. 13. Comparison of (a) H-plane and (b) E-plane principal plane far-field patterns obtained from a reference (amplitude and phase) measurement and phase retrieval. The antenna patterns with no aperture blockage (from amplitude and phase measurement) are also shown for contrast. Valid angle is $\sin(\theta_v) = 0.906$.

TABLE IV
FAR-FIELD PATTERN STATISTICS FOR THE WAVEGUIDE-FED SLOT ARRAY ANTENNA

		Blockage	
	No Blockage	*Reference*	*Phase Retrieval*
H-plane Beamwidth	5.01°	5.11°	5.12°
E-plane Beamwidth	7.90°	7.73°	7.63°
Directivity	29.68 dB	29.34 dB	29.41 dB
Average Sidelobe Level	-41.48 dB	-37.14 dB	-37.05 dB
Peak Sidelobe Level	-23.05 dB	-18.75 dB	-18.41 dB

Note: Average sidelobe level is defined to be a measure of the power in the pattern excluding a

statistics for the reference and phase retrieval cases. Pattern statistics for the case when the antenna has no blockage present are also provided for contrast. The pattern statistics confirm that the phase retrieval process has accurately reproduced the reference far-field pattern.

Microwave holographic images of the antenna aperture plane fields have been produced for both the reference and phaseless measurement cases, to determine whether the phase retrieval results could "capture" the existence of the imposed

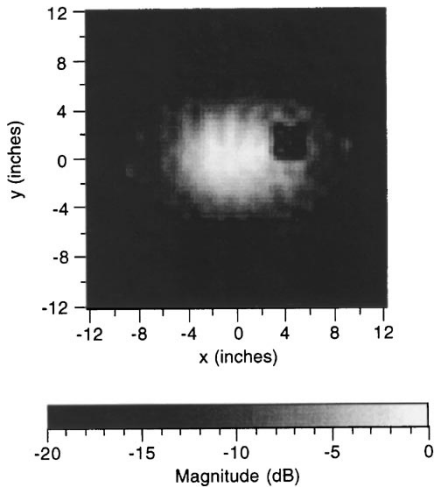

(a)

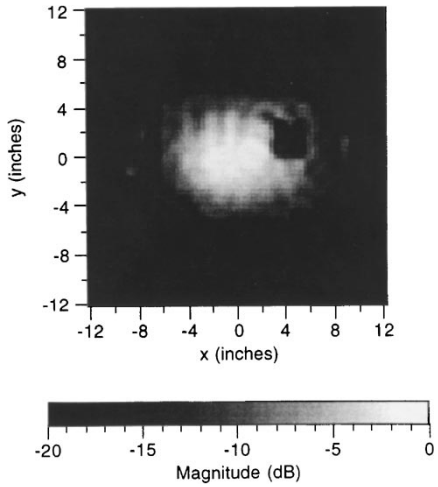

(b)

Fig. 14. Holographic image of aperture plane magnitude obtained from (a) amplitude and phase measurement and (b) phase retrieval.

aperture blockage. A comparison of the reference and phase retrieval results for the aperture plane magnitude and phase are shown in Figs. 14 and 15, respectively. The aperture blockage has been recovered accurately (size and location) although no *a priori* knowledge about its existence was assumed. In addition, the phase retrieval process has also precisely captured the magnitude and phase distribution of the AUT aperture field.

VI. CONCLUSION

A phase retrieval algorithm particularly well-suited for phaseless bi-polar planar near-field antenna measurements was presented. This algorithm employed both squared amplitude OSI and iterative Fourier techniques. The application of the described algorithm to two waveguide-fed slot array antenna phaseless measurement examples was presented. The first example focused on the phase retrieval of a near-circular aperture array antenna and the second on the phaseless diagnostics of a masked elliptical aperture array antenna. The far-field pattern and antenna aperture holographic images produced from the phase retrieval algorithm were shown to have excellent agreement with results produced using the measured near-field

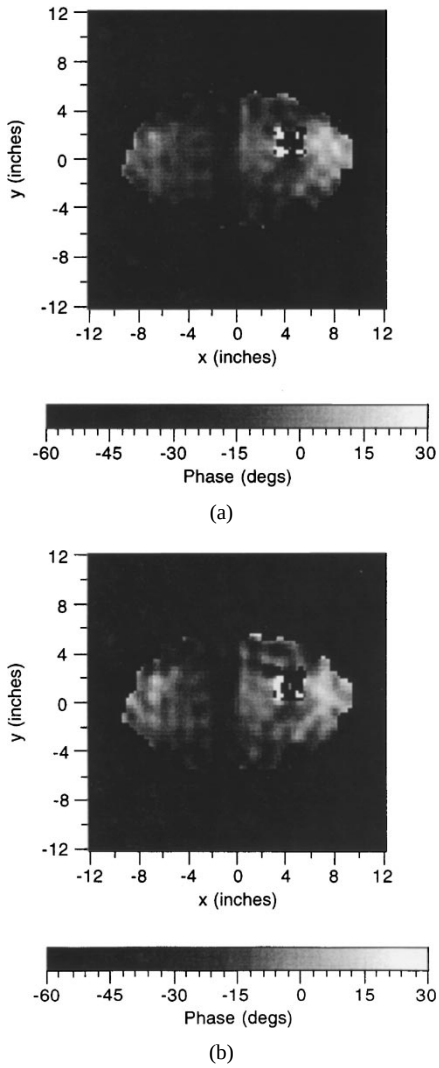

Fig. 15. Holographic image of aperture plane phase obtained from (a) amplitude and phase measurement and (b) phase retrieval.

amplitude *and* phase. These results indicate that phase retrieval methods are now becoming a mature and practical antenna measurement alternative when phase cannot be measured (or measured accurately), for example, in high-frequency antenna applications. The success of the phase retrieval algorithm, however, is dependent on many factors including, for example, the proximity of the "initial guess" to the actual solution.

REFERENCES

[1] A. D. Yaghjian, "An overview of near-field antenna measurements," *IEEE Trans. Antennas Propagat.*, vol. 34, pp. 30–45, Jan. 1986.
[2] *IEEE Trans. Antennas Propagat. (Special Issue on Near-Field Scanning Tech.)*, vol. 36, June 1988.
[3] L. S. Taylor, "The phase retrieval problem," *IEEE Trans. Antennas Propagat.*, vol. AP-29, pp. 386–391, Mar. 1981.
[4] J. R. Fienup, "Phase retrieval algorithms: A comparison," *Appl. Opt.*, vol. 21, pp. 2758–2769, Aug. 1982.
[5] R. W. Gerchberg and W. O. Saxton, "A practical algorithm for the determination of phase from image and diffraction plane pictures," *Optik*, vol. 35, pp. 237–246, 1972.
[6] D. L. Misell, "A method for the solution of the phase problem in electron microscopy," *J. Phys. D, Appl. Phys.*, vol. 6, pp. L6–L9, 1973.
[7] A. P. Anderson and S. Sali, "New possibilities for phaseless microwave diagnostics—Part I: Error reduction techniques," *Proc. Inst. Elect. Eng.*, vol. 132, pp. 291–298, Aug. 1985.
[8] T. Isernia, G. Leone, and R. Pierri, "Radiation pattern evaluation from near-field intensities on planes," *IEEE Trans. Antennas Propagat.*, vol. 44, pp. 701–710, May 1996.
[9] R. G. Yaccarino and Y. Rahmat-Samii, "Microwave antenna imaging, diagnostics, and phaseless reconstructions," *Int. J. Imaging Syst. Technol.*, vol. 8, no. 4, pp. 396–406, 1997.
[10] L. I. Williams, Y. Rahmat-Samii, and R. G. Yaccarino, "The bi-polar planar near-field measurement technique—Part I: Implementation and measurement comparisons," *IEEE Trans. Antennas Propagat.*, vol. 42, pp. 184–195, Feb. 1994.
[11] R. G. Yaccarino, L. I. Williams, and Y. Rahmat-Samii, "The bi-polar planar near-field measurement technique—Part II: Near-field to far-field transformation and holographic imaging methods," *IEEE Trans. Antennas Propagat.*, vol. 42, pp. 196–204, Feb. 1994.
[12] Y. Rahmat-Samii, L. I. Williams, and R. G. Yaccarino, "The UCLA bi-polar planar-near-field antenna-measurement and diagnostics range," *IEEE Antennas Propagat. Mag.*, vol. 37, pp. 16–35, Dec. 1995.
[13] L. I. Williams, Y. Rahmat-Samii, and R. G. Yaccarino, "A comparison of polar, thinned-polar, and linear spiral sampling using the UCLA bi-polar planar near-field measurement system," in *17th Annu. AMTA Symp. Dig.*, Williamsburg, VA, Nov. 1995, pp. 358–363.
[14] R. G. Yaccarino, L. I. Williams, and Y. Rahmat-Samii, "Linear spiral sampling for the bi-polar planar near-field antenna measurement technique," *IEEE Trans. Antennas Propagat.*, vol. 44, pp. 1049–1051, July 1996.
[15] D. M. Kerns, *Plane-Wave Scattering-Matrix Theory Antennas Antenna—Antenna Interactions*, Nat. Bureau Stand., Monograph 162, June 1981.
[16] J. J. Lee, E. M. Ferren, D. P. Woolen, and K. M. Lee, "Near-field probe used as a diagnostic tool to locate defective elements in an array antenna," *IEEE Trans. Antennas Propagat.*, vol. 36, pp. 884–889, June 1988.
[17] O. Bucci, C. Gennarelli, and C. Savarese, "Fast and accurate near-field far-field transformation by sampling interpolation of plane polar measurements," *IEEE Trans. Antennas Propagat.*, vol. 39, pp. 48–55, Jan. 1991.
[18] J. W. Goodman, *Introduction to Fourier Optics.* New York: McGraw-Hill, 1968.

Robert G. Yaccarino (S'86–M'98) was born in Howard Beach, NY, in 1963. He received the B.S. degree in electrical engineering from the University of Pennsylvania, Philadelphia, in 1985, and the M.S. degree in electrical engineering from the University of California, Los Angeles (UCLA), in 1989. He is currently working toward the Ph.D. degree in electrical engineering at UCLA.

Since 1985, he has been with the Electromagnetic Systems Laboratory of Hughes Aircraft Company (now a part of Raytheon Systems Company), El Segundo, CA, where he has been involved with the design, analysis, and measurement of passive and active antennas. His interests include antenna array analysis and pattern synthesis, the near-field measurement, imaging, radar cross section (RCS) of antennas, and the application of numerical techniques to electromagnetic radiation and scattering.

Mr. Yaccarino is the recipient of Hughes Aircraft Company Masters and Doctoral Fellowships and the IEEE Antennas and Propagation Society's 1995 Wheeler Best Applications Paper prize. He is a member of Tau Beta Pi, Eta Kappa Nu, and the IEEE Antennas and Propagation and Microwave Theory and Techniques Societies.

Yahya Rahmat-Samii (S'73–M'75–SM'79–F'85), for a photograph and biography, see p. 76 of the January 1999 issue of this TRANSACTIONS.